

SUPPORTING INFORMATION

Photonic Hypercrystals: new media for control of light-matter interaction

T. Galfsky^{1,2}, J. Gu^{1,2}, E.E. Narimanov³, and V. M. Menon^{1,2,*}

¹ Department of Physics, City College, City University of New York (CUNY), New York, USA

² Department of Physics, Graduate Center, City University of New York (CUNY), New York, USA

³ Birck Nanotechnology Center, School of Computer and Electrical Engineering, Purdue University, Indiana, USA

*corresponding author: vmenon@ccny.cuny.edu

S1. Effective permittivity and emission spectrum of CdSe/ZnS core-shell quantum dots

A metal-dielectric stack can be validly approximated by a homogenous anisotropic medium when the unit cell thickness is smaller than $\lambda/10$ and if it consists of at least 4 periods (1). In such case the parallel (x- and y-directions) and perpendicular (z-direction) permittivities of the medium with respect to the layers are given by

$$\varepsilon_x = \varepsilon_y = \rho\varepsilon_m + (1-\rho)\varepsilon_d, \quad (\text{S1})$$

$$\varepsilon_z = \frac{\varepsilon_m\varepsilon_d}{\rho\varepsilon_d + (1-\rho)\varepsilon_m}, \quad (\text{S2})$$

where ε_m and ε_d are the complex permittivities of the metal and dielectric respectively, ρ is the fill fraction of the metal in the structure

$$\rho = t_m / (t_m + t_d) \quad (\text{S3})$$

and t_m and t_d are the layer thickness of the metal and dielectric layers in a single unit cell respectively. For convenience, since $\varepsilon_x = \varepsilon_y$ we define $\varepsilon_{xy} = \varepsilon_x = \varepsilon_y$ as the permittivity component any in-plane direction (parallel to the layers). In our fabricated structure $\rho \sim 0.5$ which places the transition point for ε_{xy} at wavelength $\lambda \sim 380 \text{ nm}$.

Figure S1.a plots the real and imaginary components of the effective permittivity tensor in the xy-plane and the z-direction (see inset for schematic of the structure with direction arrows). The effective permittivity of the metamaterial was calculated using the optical constants of thin film Ag and Al_2O_3 obtain by ellipsometry measurements (using J.A. Woollam M-2000) on control samples prepared by electro-beam deposition. On the top right a schematic of the iso-frequency contour shows a hyperboloid shape which occurs when, $\varepsilon_{xy} < 0$ and $\varepsilon_z > 0$. The emission of the embedded quantum dots is chosen in order to operate in the deeply hyperbolic regime. In figure S1.b the emission spectrum of the CdSe/ZnS core-shell quantum dots is plotted.

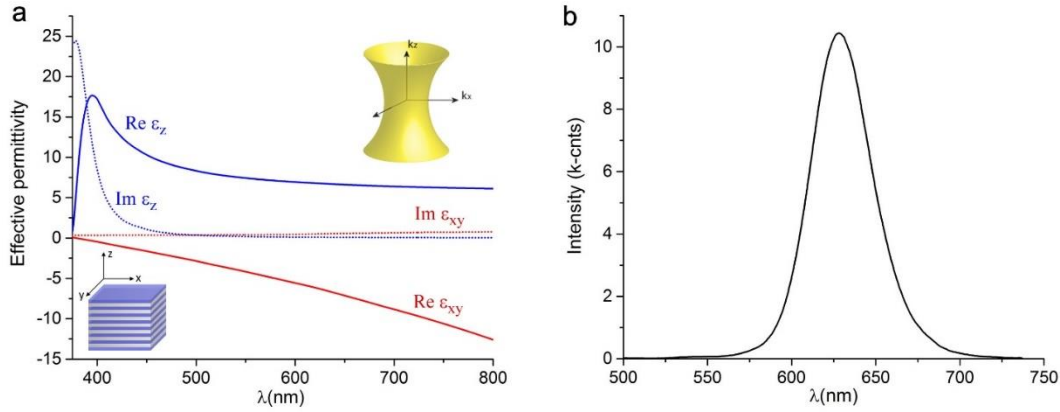


Figure S1. (a) Real and imaginary components of the effective permittivity tensor in the xy and z directions (as seen in schematic). The upper right inset sketches the shape of the iso-frequency contour for $\epsilon_{xy} < 0$ and $\epsilon_z > 0$. (b) Emission spectrum of CdSe/ZnS core-shell quantum dots used in the experiments.

S2. FDTD simulations for bandstructure and reflection

FDTD simulations were performed using commercial software Lumerical™. For bandstructure simulations scattered broadband dipole sources are placed inside a corrugated or un-patterned HMM structure surrounded by simulation region with Bloch boundary conditions. Several energy monitors distributed in the simulation region recorded the energy spectrum from a sweep of the wave-vector on the boundary conditions. Fourier transform is performed on the recorded energy spectra to obtain the bandstructure as a function of wave-vector⁵. Figure S2.a shows the simulation region with electric dipoles placed inside a 7P HMM with etched air holes of 300nm period. Figure S2.b shows the bandstructure of the corrugated film as a function of the normalized wave-vector, k_x/k_0 .

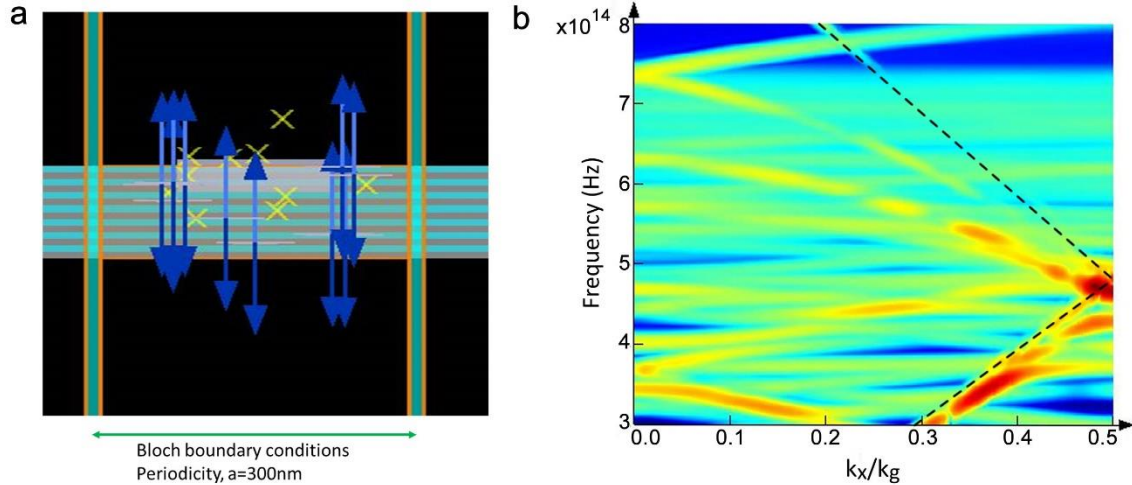


Figure S2. (a) FDTD simulation region. The blue arrows are dipoles positioned inside the HMM. The yellow X's are time monitors that measure energy as a function of simulation time. The faint grey square is an etched air grating. The distance between the horizontal green lines dictated the periodicity of the structure. (b) The simulated bandstructure of an HMM with 300nm periodic hole array. The hole diameter is 150nm.

The bandstructure simulations were supplemented by reflection simulations for various substrates. In this simulation a plane wave source is placed below the substrate at a given angle and the amount of power reflected from the structure is measured by a power monitor placed behind the plane wave source (see Fig. S3.a). The simulation uses Bloch boundary conditions to match the source angle. One crucial element to consider when running FDTD simulations of this kind is the change in source angle as a function of wavelength⁶. Since the source is broadband there's a variation in the injection angle as a function of wavelength. Higher wavelengths get injected at higher angles than the source angle for the center wavelength of the injected spectrum. If the source is tilted beyond a certain angle, the injection angle for higher frequencies can surpass 90 degrees which results in injection of evanescent waves into the simulation region⁶. We avoid this problem by keeping the source angle below that critical angle. By doing this the reflection curve is only obtained up to a certain angle which decreases as a function of wavelength. The evanescent region in our reflection figures is marked by a black semi-circle. In addition to the reflection simulations in the paper body, we present here simulations for a single silver film of 500nm thickness etched with 900nm period (Fig. S3.b) air-grating and 300nm (Fig. S3.d). These simulations were performed as an accuracy check for this method. Overlaid on the two reflection maps is the grating order dispersion for these two patterns, obtained by equating the grating equation to the wave-vector of a surface-plasmon-polariton (k_{SPP}).

$$k_{SPP} = k_0 \sin(\theta) + m \cdot k_g, \quad (\text{S4})$$

where $k_0 = 2\pi / \lambda$, and $k_g = 2\pi / a$, a is the grating period, m is the grating order. k_{SPP} was obtained from a simple Drude model for the SPP dispersion.

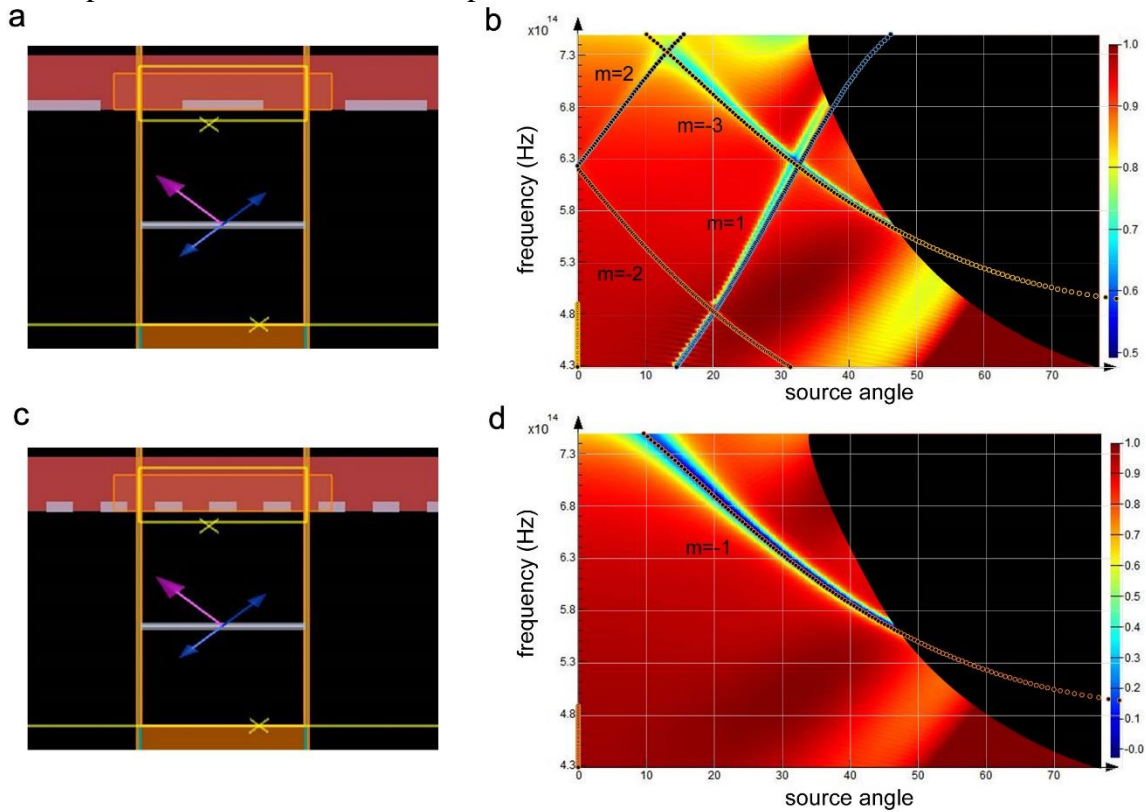


Figure S3. (a) Reflection simulation region. The source angle is swept from 0 to 45 degrees. The grey rectangle is an etched air hole with 450nm diameter. Periodicity is set to 900nm. (b) Reflection map of air-hole array of 900nm periodicity. Grating orders are overlaid on the image.

No fitting function was applied. (c) Screen grab of simulation with 300nm periodic array, hole diameter of 150nm. (d) Reflection map of air-hole array with 300nm grating. Only the $m=-1$ grating order can couple the SPP mode to free-space.

S3. FDTD Simulations of Purcell factor and electric field radiation for PHC and HMM

Enhancement in a hyperbolic medium stems from modifying the effective medium in the vicinity of the dipole emitter which is embedded inside the hyperbolic metamaterial and is an extremely near-field effect. The periodic modulation of the surface which forms the PHC only acts a small perturbation to the effective medium seen by the dipole emitter. Fig. S4a is obtained by a full 3D FDTD simulation of a dipole emitter on top of a PHC or a HMM. As seen in the graph the calculated Purcell factor is nearly the same for both HMM and PHC. Fig. S4b shows the out-coupling effect from a PHC with the correct periodicity for the center emission wavelength of our QDs (635nm). The top panel shows the electric-field emitted by a dipole oriented vertically to the layers embedded in the PHC. A horizontal dipole shows a similar effect with a lesser degree of coupling to high-k modes due to the dipoles primarily TE-polarized emission (2, 3). The vertical patterns seen in the figure are the result of scattering from the holes etched in the HMM. It is an interference effect from a single coherent source. This effect cannot be observed in experiments due to the incoherent nature of spontaneous emission of a dipole ensemble. The bottom panel shows the same dipole in a HMM. Notice most of the radiation remains trapped inside the metamaterial.

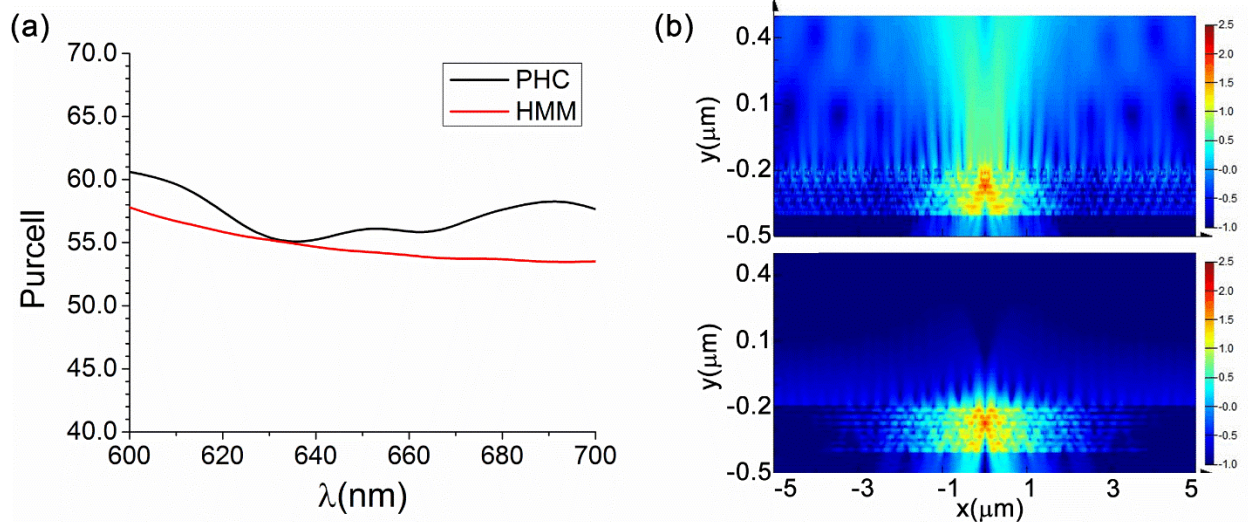


Figure S4. (a) Purcell factor as a function of wavelength for HMM (black), PHC (red). (b) TOP: electric field emitted by a vertical dipole embedded in a PHC with $a=280$ nm periodicity; BOTTOM: electric field emitted by a vertical dipole embedded in a HMM at 635nm.

S4. k-space and real-space reflection measurements for PHCs

Fourier space (k -space) images of white-light reflection from the PHCs are taken by projecting the back plane of the microscope objective lens onto the monochromator with a CCD. The k -space is imaged on 1024 x 1024 pixels CCD camera (Pixis 1024b) installed on a Princeton Instruments monochromator which allows us to resolve one of the k -space axis (x or y) as a function of wavelength.

Figure S5a, b show a k -space image in the y plane of two PHCs with the same hole radius (80nm) and different periodicity $a = 280nm$ and $a = 370nm$ respectively. Both k -space images show reduced reflection at 450-575nm range however this is an artifact of the normalization of the measurement rather than an indication of in-coupling to modes in the material. The metamaterial is composed of silver layers, a material which becomes exponentially transparent to light in the 500nm-400nm band (see paper Fig. 1c). The PHC reflection is normalized with respect to the reflection of the HMM according to the following formula:

$$R_p = (R_{HMM} - R_{PHC}) / R_{HMM} \quad (S5)$$

We must keep in mind that the PHC is achieved by removing material from the first two periods of the HMM and therefore contains a lesser amount silver than the HMM which makes it more transparent in this wavelength range. This is apparent in the normalized k -space images. The region of lower reflection seen in Fig. S5b is due to increased transmission in this range and not due to in-coupling. In contrast in Fig. S5a we see a clear dependence on angle for the wavelength range between 600-800 nm which includes the emission range of the QDs. Other PHCs show similar k -space images which gradually transitions from the image shown in Fig. S5a to the one shown in Fig. S5b with increasing period.

The relationship between out-coupling efficiency and reflection of the PHCs is demonstrated in Fig. S5c,d. In Fig. S5a we plot the real-space reflection of all the PHCs with hole radius of 80nm. Real-space reflection is taken by projecting the image-plane of a desired PHC onto the entrance slit to a spectrometer (effectively integrating over all angles in the k -space image). We see that in the range of emission of the QDs ($635nm \pm 20nm$) each PHC has a different reflection with the lowest one belonging to the PHC with periodicity, $a = 280nm$. Notice that this is a broadband effect which cannot be achieved with a regular photonic crystal defect cavity. Fig. 5b shows the emission intensity from the array of PHCs along a cutline through the center of all PHCs (taken from paper Fig. 4b). The intensity relations between different PHCs match the relations in the reflection graph. $280 > 255 > 335 > 305 > 370$.

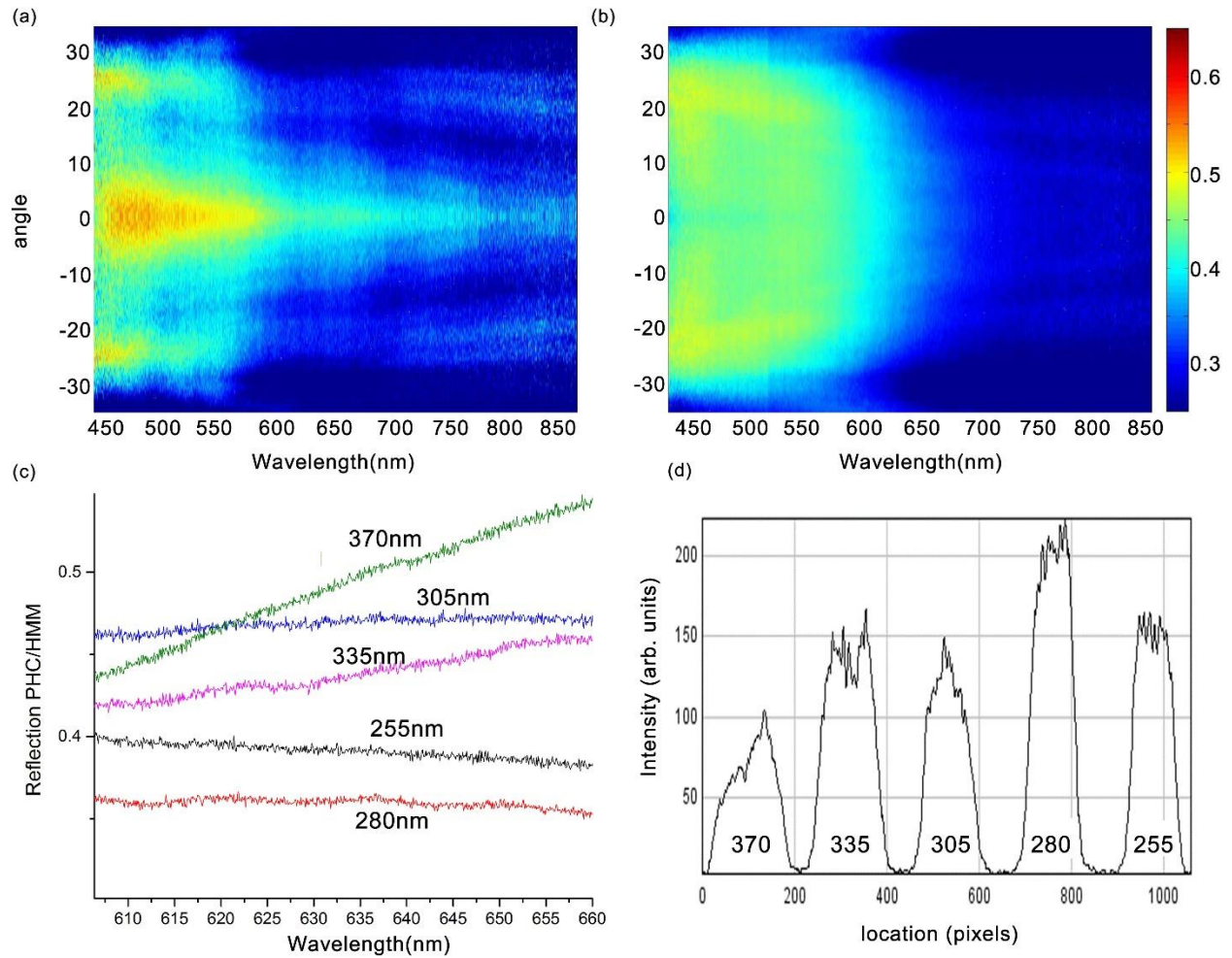


Figure S5. White-light k-space reflection measurements of (a) PHC with $a = 280\text{nm}$ and (b) PHC with $a = 370\text{nm}$. (c) Real-space reflection measurements for row of PHCs with radius 80nm and varying periodicity (labeled on graph). (d) Intensity measured along a cut-line of the photoluminescence (PL) intensity map shown in paper in Fig. 4b. Both out-coupled intensity and in-coupled white light in reflection measurement have a one-to-one correspondence in that highest PL intensity corresponds to lowest reflection of a PHC.

REFERENCES

1. Elser J, Govyadinov A a., Avrutsky I, Salakhutdinov I, Podolskiy V a. (2007) Plasmonic Nanolayer Composites: Coupled Plasmon Polaritons, Effective-Medium Response, and Subdiffraction Light Manipulation. *J Nanomater* 2007:1–8.
2. Potemkin AS, Poddubny AN, Belov P a., Kivshar YS (2012) Green function for hyperbolic media. *Phys Rev A* 86(2):023848.
3. Galfsky T, et al. (2015) Active hyperbolic metamaterials : enhanced spontaneous emission and light extraction. *Optica* 2(1):62–65.